Information content of data measured with a multiple-field-of-view lidar

Igor Veselovskii, Michail Korenskii, Vadim Griaznov, David N. Whiteman, Matthew McGill, Gilles Roy, and Luc Bissonnette

Lidars with multiple fields of view (MFOVs) are promising tools for gaining information on cloud particle size. We perform a study of the information content of MFOV lidar data with the use of eigenvalue analysis. The approach we have developed permits an understanding of the main features of MFOV lidars and provides a way to relate the accuracy of particle size estimation with the measurement uncertainty and the scattering geometry such as the cloud-base height and the lidar sounding depth. Second-order scattering computations are performed for an extended range of particle sizes and for a wide range of lidar fields of view (FOVs). The results obtained allow us to specify the areas of possible applications of these lidars in cloud studies. Comparison of results obtained with polarized and cross-polarized scattered components demonstrate that the cross-polarized signal should provide a more stable retrieval and is preferable when double scattering is highly dominant. Our analysis allows for the estimation of the optimal number of FOVs in the system and their angular distribution, so this work can be a useful tool for practical MFOV lidar design.

OCIS codes: 280.0280, 280.1100, 280.3640, 290.4210.

1. Introduction

Clouds are one of the main factors influencing planetary climate. This influence depends on the heights and distribution of clouds and on their radiative properties, which in turn are determined by cloud microphysical parameters. Thus developing new types of instrumentation for the remote monitoring of cloud parameters, such as vertical profiles of particle mean radius and concentration is a task of high priority in modern climate study. One of the ways to monitor these parameters remotely is to examine the multiple scattering of laser radiation because the angular distribution of multiply scattered radiation contains information on the particle size distribution. Among different approaches exploiting this principle,[1] the tools of particular interest are lidars with multiple fields of view (MFOV). Progress made during the past decade by the Valcartier research group[2–5] allows us to consider MFOV lidar as a powerful instrument for cloud study. However, some important questions concerning the application of this technique remain to be clarified. The questions to answer before constructing a MFOV lidar include

- How many fields of view (FOVs) should be used, keeping in mind, that each additional FOV will make a system more expensive and complicated?
- What interval of FOV should be used and how should the FOVs be distributed inside this interval?
- What range of particle size can be retrieved, and how does this range depend on cloud height, lidar sounding depth, and measurement uncertainty?

These questions, in principle, can be answered using extensive numerical simulations for different combinations of particles and lidar parameters. However, such an approach is extremely time consuming and much of the information obtained is irrelevant for establishing relationships between different parameters and for clarifying their dependence on measurement accuracy.

An alternative approach to the problem was suggested in a recent publication concerning the re-

I. Veselovskii (igorv@quadra.ru), M. Korenskii, and V. Griaznov are with the Physics Instrumentation Center of the General Physics Institute, Troitsk, Moscow Region 142190, Russia. D. N. Whiteman (david.whiteman@gsfc.nasa.gov) and M. McGill are with the NASA Goddard Space Flight Center, Greenbelt, Maryland 20771. G. Roy (gilles.roy@drev.dnd.ca) and L. Bissonnette are with Defence Research and Development Canada–Valcartier, 2459 Boul, Pie-XI Nord, Val-Belair, Quebec G3J 1X5, Canada.

Received 3 January 2006; revised 18 March 2006; accepted 28 April 2006; posted 1 May 2006 (Doc. ID 66896).

0003-6935/06/266839-10$15.00/0

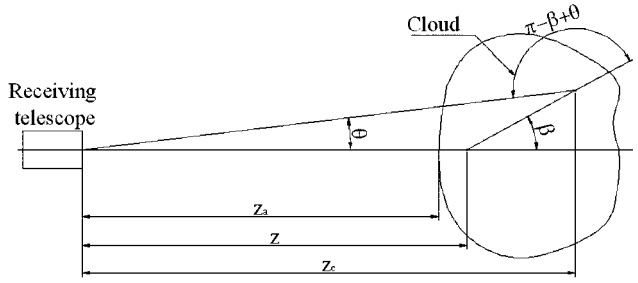

Fig. 1. Geometry for the calculation of the scattered power at the entrance of a receiving telescope in the framework of a double-scattering approximation.

trieval of particle parameters from multiwavelength aerosol lidar measurements.[6] The method is based on the consideration of the information content of lidar data using eigenvalue analysis. This approach gives only estimations, but it allows for obtaining the big picture and provides answers to the questions formulated above. Thus in the present paper, we apply the eigenvalue technique to generate predications of MFOV lidar performance.

2. Methodology

The MFOV lidar particle size retrieval method is based on the measurement of the angular distribution of multiply scattered laser radiation. The calculation of the angular energy distribution for an arbitrary number of scattering orders can be performed using approximate models[7] or Monte Carlo methods.[8] But we should point out that our main interest is in solving the inverse problem, i.e., the retrieval of the particle size distribution (PSD) from the measured angular spectrum, which can only be done in a straightforward manner using a double-scattering approximation.[3,4] For this reason, we will limit our consideration only to second-order scattering events, though our proposed technique may also be used for higher scattering orders. Thus the results obtained will be valid for optically thin aerosol layers and for small sounding depths in clouds. For the calculation of the angular spectrum of doubly scattered radiation, we use the geometry suggested in Refs. 3 and 4, which is shown in Fig. 1. The laser radiation is scattered forward at a height z located between cloud base z_a and height z_c, where the radiation is backscattered. We do not consider the alternative scenario, when backscattering occurs first followed by forward scattering, because it leads to the same results as a consequence of the reciprocity theorem.[9,10]

The essence of the MFOV lidar technique is the measurement of the scattered power $S(\theta)$ as a function of receiver FOV. It should be noted that in Fig. 1, the angle θ corresponds to one half of the lidar FOV. Changes of particle size distribution lead to variations of $S(\theta)$. If the functions $S_i(\theta)$ corresponding to different PSDs are linearly independent, then the retrieval of the PSD becomes possible.

We assume that the laser beam divergence θ_{las} is small and that the scattered power originating from single-scattering events is concentrated inside the smallest FOV θ_{min}. It should be noted that this constraint is fulfilled only for small receiver apertures D such that $1/2(\theta_{las} + D/z_c) < \theta_{min}$. We also assume that the cloud is homogeneous in extinction and droplet size and that the time delay of the scattered photons at different FOVs is negligible. In lidar measurements, the FOV range $[\theta_{min}, \theta_{max}]$ is usually divided into several concentric intervals, and the scattered power inside these intervals is integrated by a detector. Scattered power in the FOV interval $\Delta\theta_i = \theta_{i+1} - \theta_i$ can be calculated as[3,4]

$$S(z_c, \Delta\theta) = S_0 e^{-2\alpha(z_c - z_a)} \frac{2}{z_c^2} \int_{z_a}^{z_c} \int_{0}^{2\pi} \int_{\beta_j}^{\beta_{j+1}} [\alpha(z) P(r, \beta)] \times [\alpha(z_c) P(r, \beta_{back})] \sin\beta \, d\beta \, d\phi \, dz. \quad (1a)$$

The factor 2 in front of the integral follows from the reciprocity theorem; S_0 is a range-independent constant; α is the extinction coefficient; $P(r, \beta)$ and $P(r, \beta_{back})$ are the values of the phase function for the forward-, β, and backward-scattering angles, $\beta_{back} = \pi - \beta + \theta$, for a particle of radius r; z_a is the range to the cloud base; z_c is the sounding range; the quantity $[\alpha(z)P(r, \beta)]$ represents the forward-scattering coefficient while $[\alpha(z_c)P(r, \beta_{back})]$ represents the backscattering coefficient; and ϕ is the azimuthal angle ranging from 0 to 2π. From Fig. 1, the scattering angle β is easily related to θ via the relation $\tan\beta = z_a \tan\theta/(z_c - z)$. Next, we write the assumed homogeneous extinction coefficient α as a function of the particle size distribution $f(r)$, i.e., $\alpha \equiv \int_{r_{min}}^{r_{max}} f(r) Q(r) \pi r^2 dr$, where $Q(r)$ is the scattering efficiency set equal to 2 in the approximation of particles larger than the wavelength. After integrating over the azimuthal angle and using the definition of the extinction coefficient, Eq. (1a) becomes

$$S(z_c, \Delta\theta) = S_0^* \frac{e^{-2\alpha(z_c - z_a)}}{z_c^2} \int_{r_{min}}^{r_{max}} f(r) r^2 \int_{z_a}^{z_b} \int_{\beta_j}^{\beta_{j+1}} P(r, \beta) \times [\alpha(z_c) P(r, \beta_{back})] \sin\beta \, d\beta \, dz \, dr, \quad (1b)$$

where S_0^* is a constant containing all the fixed parameters.

The main information about particle size (if we do not consider polarization effects) is contained in the forward peak of the scattering phase function.[11] To simplify the analysis, $P(r, \beta_{back})$ in some computations is assumed isotropic (angle independent). It will be shown that this approximation does not influence the results much. The phase function for scattering in the forward direction $P(r, \beta)$ is calculated through Mie theory.[12]

For the analysis of the information content, a more representative characteristic is $s(\theta) = dS(\theta)/d\theta$, which describes the scattered power measured inside an elementary angle $d\theta$ and allows us to determine which FOV intervals are the most sensitive to vari-

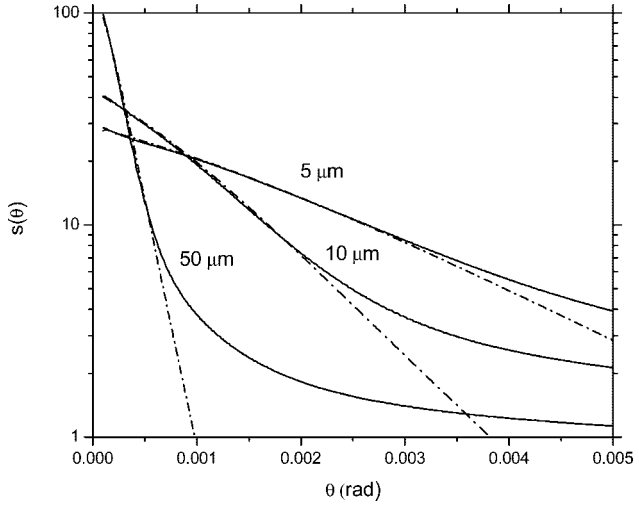

Fig. 2. Angular distributions of scattered radiation power over the telescope FOV. Calculations are performed for a lognormal particle size distribution with a modal radius of $r_0 = 5$, 10, and 50 μm. The cloud base is at $z_a = 500$ m; the sounding depth is at $\Delta z = 50$ m. Dashed–dotted curves show the results obtained with the Gaussian approximation of $P(r, \beta)$.

ations of particle parameters. Figure 2 shows the function $s_i(\theta)$ calculated for lognormal size particle distributions with modal radii of $r_{0i} = 5$, 10, 50 μm, sounding depth of $\Delta z = z_c - z_a = 50$ m, and cloud base of $z_a = 500$ m. Phase function $P(r, \beta_{\text{back}})$ is assumed to be isotropic. The half-angle FOV is varied over the interval $0.1 < \theta < 5$ mrad. Here and in all calculations, the dispersion factor is taken as $\ln \sigma = 0.35$, the refractive index as $m = 1.33$, and the laser wavelength as $\lambda = 1.06$ μm. The distributions are normalized to keep $\int_{\theta_{\min}}^{\theta_{\max}} s(\theta)\mathrm{d}\theta = 1$. The dashed–dotted curves in Fig. 2 show the results obtained with the Gaussian approximation of the forward-scattering peak[7]; this approximation will be used in Fig. 3(a) to illustrate the main features of the considered scattering geometry. For large θ, the Gaussian approximation leads to a faster drop of the scattered intensity compared to the Mie formulas. With the increase of altitude z_a, the angular distributions $s_i(\theta)$ become narrower, and therefore useful information is contained primarily at small FOVs. The implementation of very small FOVs demands fine laser beam alignment and high mechanical stability of the steering optics. To diminish these problems, it is desirable to work with long-wavelength radiation because the width of the forward-scattering peak [and so $s(\theta)$] is determined by the ratio λ/r. However, the use of radiation wavelengths longer than 1.06 μm introduces additional difficulties at the detection end because of the limitations in detector technologies. Consequently, in the model of this paper, we consider only the 1.06 μm wavelength. The angular distributions $s_i(\theta)$ also depend on the sounding depth Δz. For the considered geometry, an increase in sounding depth is equivalent to a decrease in z_a since, for $\Delta z \ll z_a$, $s(\theta)$ is a function of the ratio $\eta = \Delta z/z_a$.

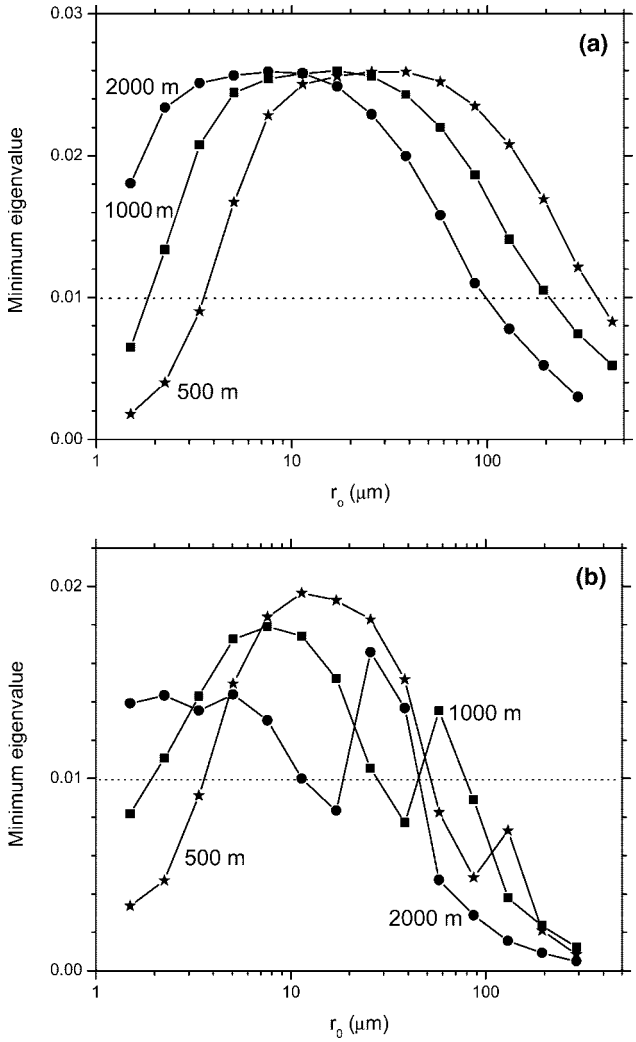

Fig. 3. Dependence of the minimum eigenvalue on particle size. Calculations are performed for $z_a = 500$, 1000, 2000 m and $\Delta z = 50$ m using (a) Gaussian approximation and (b) Mie formulas for the computation of $P(r, \beta)$. FOVs are in the interval $\theta_{\min} = 0.25$, $\theta_{\max} = 5$ mrad.

3. Numerical Test for the Linear Independence of Optical Data

For the sake of the analysis we need a quantitative criterion that characterizes the linear independence of the angular spectrum of $s_i(\theta)$ and that can be related to the measurement error ε. As shown in Ref. 13, the set $s_i(\theta)$ may be considered as linearly independent if $l_{\min} > \varepsilon^2$, where $l_{\min}$ is the minimum eigenvalue of the covariance matrix $\mathbf{C}$ with elements $c_{i,j} = \int_{\theta_{\min}}^{\theta_{\max}} s_i(\theta) s_j(\theta)\mathrm{d}\theta$.

The test for linear independence was done for a set of $s_i(\theta)$, obtained for lognormal size distributions with modal radii r_{0i}. The dispersion factor was assumed to be the same for all distributions and equal to $\ln \sigma = 0.35$, but, in general, the variation of dispersion may also be included in the modeling. To perform the test, the first element $s_1(\theta)$ (corresponding to the PSD with r_{01}) is compared with every element from the rest of the set. The procedure is then repeated for the

second, the third, and every following element. For each pair, we form the 2×2 covariance matrix and determine the corresponding minimum eigenvalue $l_{\min}$. If the smallest $l_{\min}$ for all pairs fulfills the requirement $l_{\min} > \varepsilon^2$, the respective data set is linearly independent. For the comparison of eigenvalues with relative measurement error, the correct normalization of the elements is essential. All elements are normalized to keep $\int s_i^2(\theta)\mathrm{d}\theta = 1$.

A. Influence of the Scattering Geometry on Retrieval Accuracy

The accuracy of particle size estimation depends on the scattering geometry, i.e., on cloud base z_a and sounding depth Δz. The lidar FOV can be presented as a superposition of concentric rings of $\Delta\theta_i$ width in the $[\theta_{\min}, \theta_{\max}]$ interval. These rings can be considered as a set of detectors, and the number of such ring FOVs is determined only by the step $\Delta\theta$ of the calculation. Thus we suggest that the lidar has an unlimited number of FOVs, so the distribution $s_i(\theta)$ can be determined with any desirable precision. The results obtained will define the upper limit of the accuracy that can, in principle, be attained with this kind of instrument. The dependence of the minimum eigenvalue $l_{\min}$ on particle size for different cloud-base heights is shown in Fig. 3. The eigenvalues are calculated for the intervals $[r_{01}, r_{0i}]$ with $r_{01} = 1$ μm in all computations. For every value of r_{0i}, the eigenvalues are calculated by comparing the corresponding element $s_i(\theta)$ with elements $s_1(\theta), \ldots, s_{i-1}(\theta)$ of the set, as described in the previous section. The minimum of these eigenvalues $l_{\min}$ is plotted on the graph. The calculations were performed for $z_a = 500$, 1000, 2000 m and $\Delta z = 50$ m. The FOVs are included in the interval $\theta_{\min} = 0.25$ mrad, $\theta_{\max} = 5$ mrad. It is desirable to keep $\theta_{\min}$ as small as possible because small angles contain information about large particles and particles at high altitudes. Constraints on the quality and cleanness of the collecting optics as well as on the laser beam quality make $\theta_{\min} = 0.25$ mrad a reasonable choice (recall that the angle θ corresponds to one half the lidar FOV). On the other hand, the experience of MFOV lidar operation in Valcartier[3,4] shows that the use of FOVs larger than 10 mrad makes the background signal above acceptable levels. It also introduces problems related to the acceptance angles of the filters and polarizers.

The minimum eigenvalue depends on the step width of the radius variation $\Delta r_{0_i} = r_{0i} - r_{0i-1}$. The larger the Δr_0, the more independent the distributions $s_i(\theta)$; thus this value is a measure of the possible radius resolution. The variation of r_0 may be performed with a constant step size, but more representative is the situation when the step size is taken as a fraction of r_0. Then, the radius resolution may be estimated as $\Delta r_{0_i}/r_{0i}$. For the curve shown in Fig. 3, $r_{0i} = 1.5 r_{0i-1}$. Thus the step width is $\Delta r_{0i} = r_{0i}/3$, and the corresponding accuracy of the radius estimation is ~30%. The dashed line shows the level corresponding to a measurement accuracy of $\varepsilon = 10\%$. Hence only radii for which $l_{\min} > \varepsilon^2$ may be retrieved.

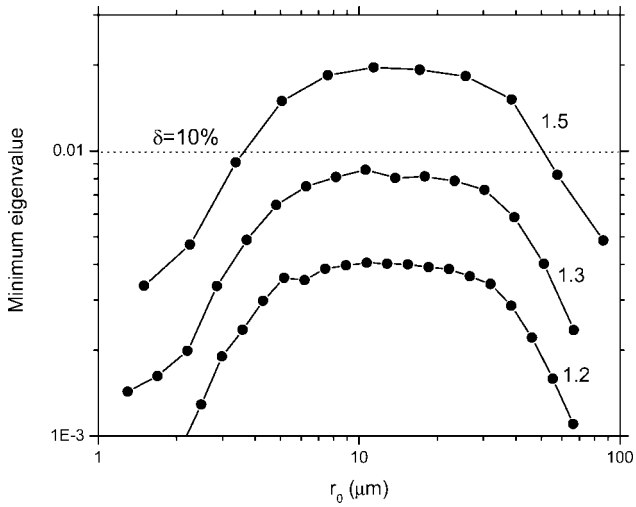

Fig. 4. Estimation of the accuracy of size retrieval with the use of MFOV lidar. The radius of the particles is varied as $r_{0i} = k r_{0i-1}$. Calculations are performed for $k = 1.5$, 1.3, 1.2; $z_a = 500$ m, $\Delta z = 50$ m.

The results in Fig. 3(a) are calculated with the Gaussian approximation of $P(r, \beta)$. Though this approximation is not very satisfactory for large θ, it is convenient to illustrate the influence of the scattering geometry on the retrieval results. Figure 3(a) shows that the rise of z_a shifts the range of stable retrieval to smaller particles. As we have already mentioned, the increase of the sounding depth Δz is equivalent to the decrease of z_a, so increasing Δz allows for the retrieval of large particles at high altitudes. The use of Mie formulas for $P(r, \beta)$ leads to a more complicated behavior of $l_{\min}(r_{0i})$ compared with the Gaussian approximation, as shown in Fig. 3(b). Still the main tendency is the same: The rise of the cloud base shifts the region of stable retrieval to smaller radii. For large Δz, the integral in Eq. (1) from z_a to z_c is determined mainly by the forward-scattering peak, so the results obtained with the Gaussian and Mie are quasi similar.

As we have already mentioned, the radius resolution of the method can be estimated by performing calculations with different steps of radius variation Δr. The calculation results are presented in Fig. 4. The particle radius is varied as $r_{0i} = k r_{0i-1}$, and for $k = 1.5$, 1.3, and 1.2, the accuracies of radius estimation $\Delta r_0/r_{0i}$ are ~33%, 23%, and 16%, respectively. As we can see, for $\varepsilon = 10\%$ and the chosen FOV range, the condition $l_{\min} > \varepsilon^2$ is fulfilled for $k > 1.3$. Hence even if a large number of FOVs are available, the realistic resolution of the retrieved particle size distribution for a 10% measurement error cannot be better than ~30%.

One of the important questions arising in the design of a MFOV lidar is the range of the required FOVs needed to provide the retrieval of the particle size distribution inside the chosen range of radii at the chosen altitude. A simple way of estimating the

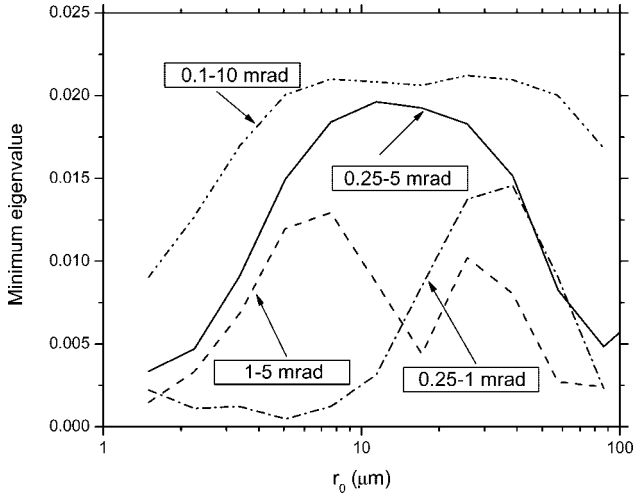

Fig. 5. Illustration of the influence of the FOV range on the interval of particle sizes that can be retrieved. Calculations are performed for θ in the intervals 0.25–5, 0.25–1, 1–5, and 0.1–10 mrad; $z_a = 500$ m, $\Delta z = 50$ m.

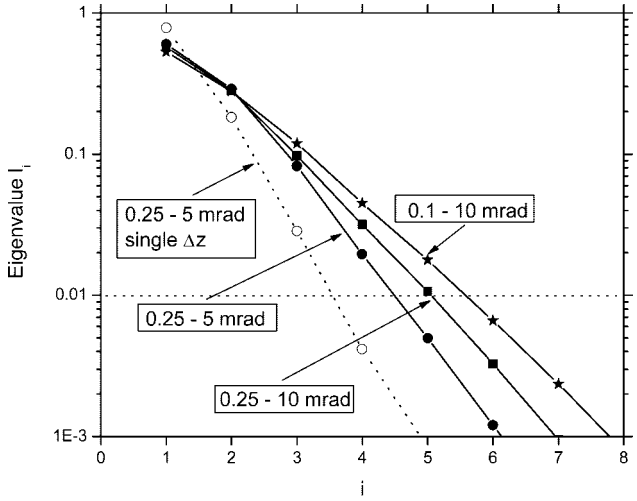

Fig. 6. Information content of MFOV lidar data for different intervals of θ: 0.25–5, 0.25–10, and 0.1–10 mrad. The dotted curve shows the results for the single value of Δz.

desired FOVs range is presented in Ref. 11. In general, large FOVs command the retrieval of small particles, and small FOVs are responsible for the retrieval of large particles, as illustrated by Fig. 5. Calculations in this figure are shown for the θ intervals of 0.25–5, 0.25–1, 1–5, and 0.1–10 mrad. Comparing the results obtained for the 1–5 and 0.25–5 mrad ranges, we can see that the extension of the FOV range toward small θ improves the estimation of both the small and large particles. Increasing the θ range up to 0.1–10 mrad further stabilizes the retrieval, but as has already been mentioned, the design of lidar with such a FOV range is a complicated task.

B. Estimation of the Required Number of Fields of View

Up to now we have suggested that the lidar has an unlimited number of FOVs. However, for practical application, it is important to know how many FOVs are needed to properly represent the angular distributions. This means that we have to investigate the degree of independence of the points of the curves $s_i(\theta)$. Alternately, we need to determine how many independent pieces of information are contained in the variations of $s(\theta)$ resulting from changes in the particle size distribution at different sounding depths. Such an analysis again rests upon the calculation of the eigenvalues l_i of the covariance matrix. The details for the use of this approach may be found in Refs. 6 and 13. For the lognormal size distributions with modal radii $r_{01}, \ldots, r_{0N}$ (in the 1–200 μm range) the corresponding angular distributions $s_i(\theta), \ldots, s_N(\theta)$ are calculated for a fixed $z_a = 1000$ m and a set of $\Delta z_1, \ldots, \Delta z_M$ (in the 50–200 m range); hence a $MN \times MN$ covariance matrix with elements $c_{ij} = \int_{\theta_{\min}}^{\theta_{\max}} s_i(\theta) s_j(\theta) \mathrm{d}\theta$ is constructed. For example, if we consider particles with different radii ($N = 14$) and different sounding depths ($M = 10$), we have to construct a matrix of 140×140 size. The number of characteristic patterns (independent pieces of information) is determined by the number of eigenvalues for which $l_i > \varepsilon^2$.

Figure 6 illustrates the information content of $s(\theta)$ data. The eigenvalues l_i are plotted as a function of their order number i. In these simulations, three FOV intervals were tested: 0.25–5, 0.25–10, and 0.1–10 mrad. The larger the range of θ considered, the more information contained in the variations of the angular distributions, but for 10% measurement accuracy, even the $0.1 < \theta < 10$ mrad interval contains no more than six independent pieces of information. For comparison, the same figure shows the result obtained when only one sounding depth $\Delta z_1 = 50$ m is considered. In this situation, for the FOV interval 0.25–5 mrad, we have only three eigenvalues above 0.01. Thus the resulting number of independent pieces of information gives us the required number of FOVs to account for the variations of the particle parameters at different altitudes. This number of FOVs should be enough to pick up the main part of the information, which is in principle available from the MFOV lidar.

The next question arising is how these FOVs should be distributed over the angular range. To answer this question, the interval $(\theta_{\min}, \theta_{\max})$ was split for several concentric rings with $\theta_{i-1} < \theta < \theta_i$. The scattered power inside every ring is calculated as

$$S_i = \int_{\theta_{i-1}}^{\theta_i} s(\theta) \mathrm{d}\theta.$$

When testing different types of FOV distributions, we try to keep $l_{\min}$ as high as possible to provide stable parameter retrieval, but at the same time, it is desirable to avoid strong variations of S_i, because the dynamic range of the lidar receiving systems is limited. The numerical simulations performed for different altitudes and sounding depths Δz demonstrate

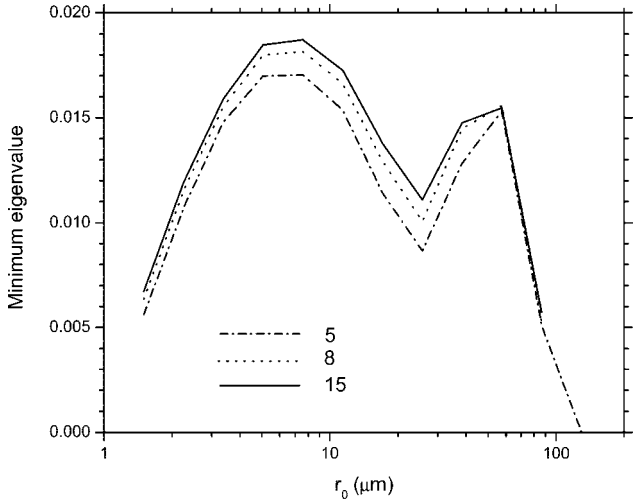

Fig. 7. Minimum eigenvalues calculated for 5, 8, and 15 FOVs distributed in the 0.25–5 mrad range with a log-equidistant law; $z_a = 1000$ m, $\Delta z = 50$ m.

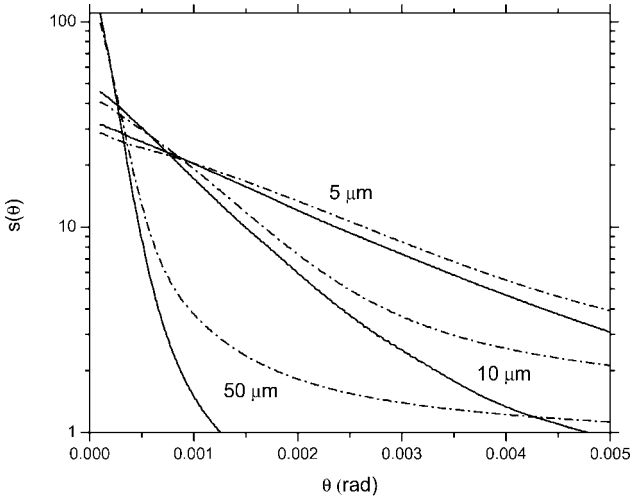

Fig. 8. Angular distribution of scattered radiation power for $r_0 = 5$, 10, and 50 μm when the phase function in the backward direction is calculated through Mie formulas. The cloud base is at $z_a = 500$ m, and the sounding depth is at $\Delta z = 50$ m. Dashed–dotted curves show the results for isotropic $P(r, \beta_{back})$.

that optimal results are obtained when the θ_i are distributed at equidistant steps on a logarithmic scale.

Figure 7 compares results obtained when 5, 8, and 15 FOVs in the 0.25–5 mrad range are used. In agreement with Fig. 6, increasing the number of FOVs beyond five does not significantly change the eigenvalues. Results in Fig. 7 were obtained for $z_a = 1000$ m and $\Delta z = 50$ m, but simulations performed for other heights and sounding depths lead to a similar conclusion: Five to six FOVs pick up the main part of all available information.

C. Consideration of the Scattering Phase Function in the Backward Direction

Up to this point, we have assumed that the scattering phase function in the backward direction is isotropic. Such an assumption is reasonable if only small FOVs are considered. To check if this limitation introduces serious errors, we performed the same numerical simulations using the true shape of $P(r, \beta_{back})$ calculated through Mie formulas. Figure 8 shows the angular distributions $s_i(\theta)$ obtained for the isotropic $P(r, \beta_{back})$ and for the backward-scattering phase function calculated through Mie theory. These distributions are quite similar for small particles, but for large r_0, the scattered power for real phase functions goes down with the rise of θ much faster than for the isotropic one. Nevertheless, this difference does not have influence much on the obtained results of the information content, as shown in Fig. 9. This finding has a simple physical interpretation: The difference in $s(\theta)$ behavior at wide θ is essential only for small particles, but as it follows from Fig. 8, the angular distribution of scattered power from small particles is the same for both types of $P(r, \beta_{back})$.

D. Use of the Cross-Polarized Lidar Signal

We have considered total scattering (the sum of both parallel and perpendicular polarizations). Additional information about particle properties can be obtained when the parallel and perpendicular polarization components are separated in the receiver. The potential of such polarization-sensitive detection for particle sizing was first demonstrated by Roy *et al.*[4] In this section, we will apply the previously described eigenvalue technique to analyze the improvement when a cross-polarized signal is used.

For the calculation of the parallel $[S_{\parallel}(\theta)]$ and perpendicular $[S_{\perp}(\theta)]$ components, the following expressions should be added as multiplicative terms to the backscattering phase function $P(r, \beta_{back})$ in the integral in Eq. (1b), i.e., $1/[1 + \delta(r, z)]$ and $\delta(r, z)/[1 + \delta(r, z)]$, respectively. Here, $\delta(r, z)$ is the ratio of

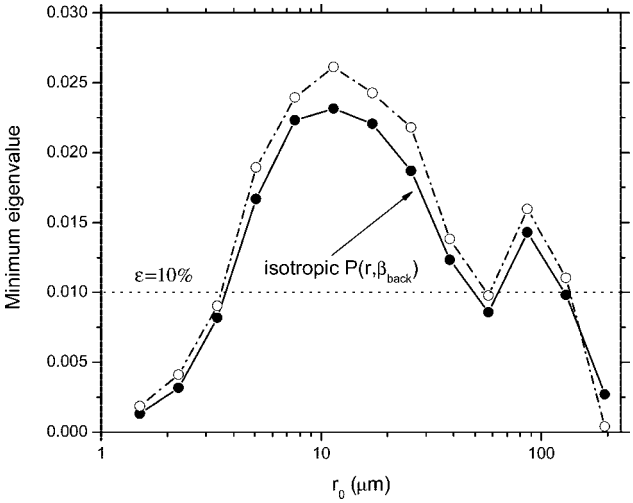

Fig. 9. Dependence of the minimum eigenvalue on particle size when the phase function in the backward direction $P(r, \beta_{back})$ is isotropic (solid symbols) and calculated through Mie formulas (open symbols). $z_a = 500$ m, $\Delta z = 50$ m.

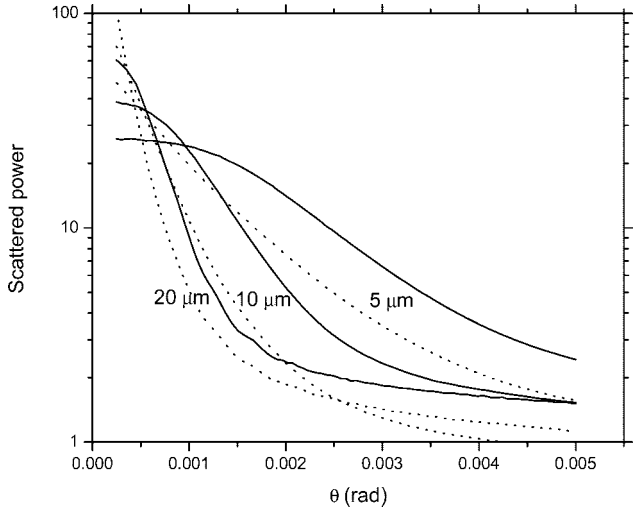

Fig. 10. Angular distributions of the cross-polarized component $s_\perp$ power (solid curves) for $r_0 = 5$, 10, and 20 μm. Dotted curves show the corresponding results for polarized components $s_\parallel$. Distributions are normalized to keep $\int_{\theta_{\min}}^{\theta_{\max}} s_{\perp,\parallel}(\theta)\mathrm{d}\theta = 1$. $z_a = 1000$ m, $\Delta z = 50$ m.

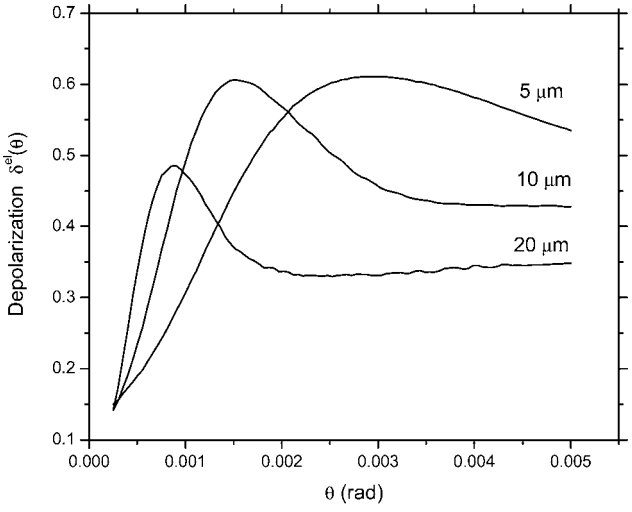

Fig. 11. Angular dependence of the depolarization $\delta^l(\theta) = s_\perp/s_\parallel$. Calculations are performed for lognormal particle size distributions with $r_0 = 5$, 10, and 20 μm; $z_a = 1000$ m, $\Delta z = 50$ m.

the perpendicular to the parallel component of the field scattered by a particle of radius r, i.e.,

values of the covariance matrix are plotted against their number. For 10% measurement uncertainty, the perpendicular signal contains about six independent components while the total signal contains less

$$\delta(r,\ z) = \frac{P_2(r,\ \beta_{\mathrm{back}})\cos^2\beta_{\mathrm{back}} - 2P_3(r,\ \beta_{\mathrm{back}})\cos\beta_{\mathrm{back}} + P_1(r,\ \beta_{\mathrm{back}})}{3P_2(r,\ \beta_{\mathrm{back}})\cos^2\beta_{\mathrm{back}} + 2P_3(r,\ \beta_{\mathrm{back}})\cos\beta_{\mathrm{back}} + 3P_1(r,\ \beta_{\mathrm{back}})}, \tag{2}$$

where P_1, P_2, P_3 are the elements of the Muller matrix[4,14] and β_{back} is the angle of the backward scattering.

For our analysis, we again consider $s_\parallel = \mathrm{d}S_\parallel/\mathrm{d}\theta$ and $s_\perp = \mathrm{d}S_\perp/\mathrm{d}\theta$. All computations in this section are performed through Mie formulas for the forward- and backward-scattering phase functions. Figure 10 shows the angular distributions of the perpendicular component for different r_0. For the sake of comparison, the same figure shows the corresponding distributions for the parallel component. The angular distribution of the total scattering $s(\theta)$ is determined mainly by the diffraction forward peak of the scattering phase function, while the cross-polarized signal depends on both the forward and backward peaks; hence it should be more informative. The distributions $s_\perp(\theta)$ are shifted toward larger θ to compare with $s_\parallel(\theta)$; thus $\theta_{\min}$ can be increased, and the problem of single- and multiple-scattering separation becomes less severe. Figure 11 shows the depolarization $\delta^{\mathrm{el}} = s_\perp/s_\parallel$ in each elementary ring dθ for the same values of r_0 as in Fig. 10. For small θ, the depolarization drops down to zero, but for larger θ it reaches a maximum whose position depends on the chosen r_0.

To estimate the number of independent pieces of information in the $s_\perp(\theta)$ variations, we perform the same analysis as in Section 3. In Fig. 12, the eigenvalues than five. To compare the particle sizes that can be retrieved with the use of different polarization components, Fig. 13 shows the minimum-eigenvalue curves obtained with $s_\parallel$ and $s_\perp$; calculations are per-

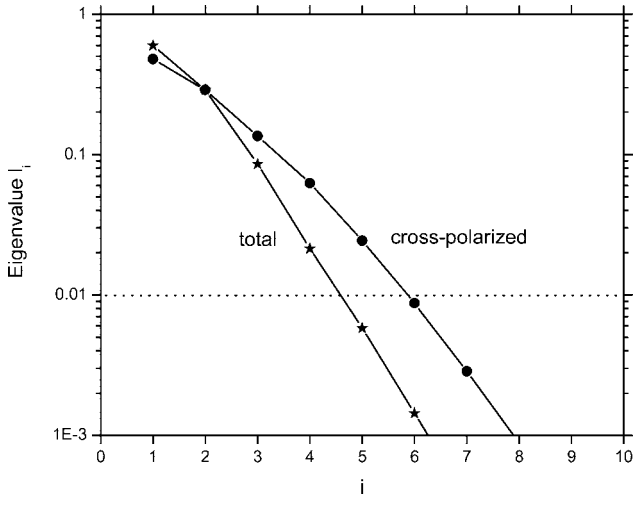

Fig. 12. Comparison of the information content of the total (sum of both polarization components) and cross-polarized (perpendicular) lidar return. Calculations are performed for the interval $0.25 < \theta < 5$ mrad.

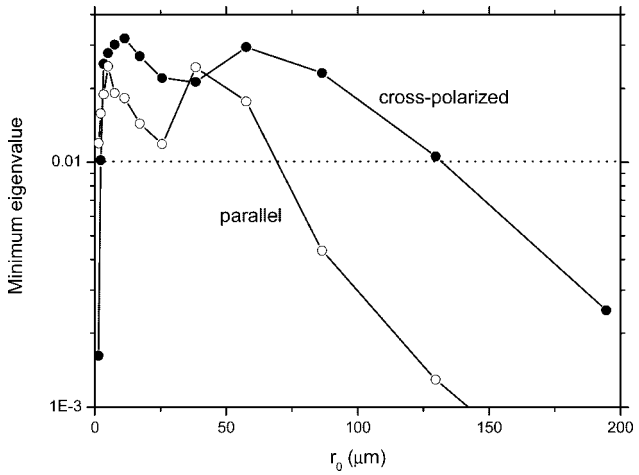

Fig. 13. Dependence of the minimum eigenvalue on particle size for the parallel and cross-polarized components. Eight FOVs are log-equidistantly distributed over the 0.25–5 mrad range; $z_a = 1000$ m, $\Delta z = 50$ m.

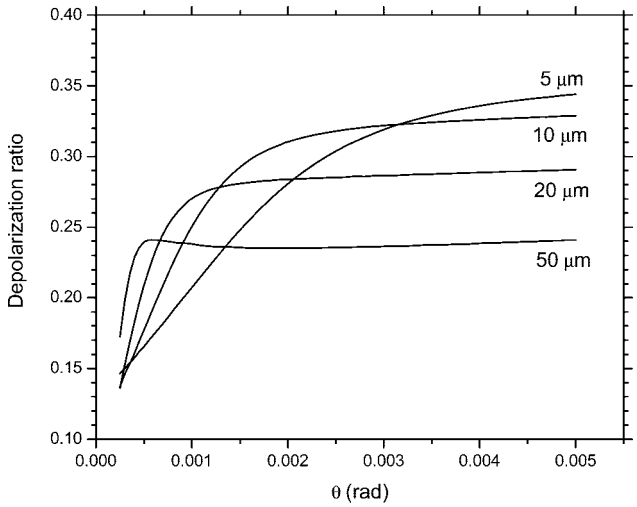

Fig. 15. Depolarization ratio $S_\perp/S_\parallel$ as a function of the FOV angle θ. Calculations are performed for $r_0 = 5$, 20, 10, 50 μm; $z_a = 1000$ m, $\Delta z = 50$ m.

formed for eight FOVs distributed log-equidistantly over the 0.25–5 mrad range. The eigenvalues obtained for $s_\perp$ are higher than for $s_\parallel$, which promises more stable retrieval.

When considering the depolarization of laser radiation by multiple scattering, it is also useful to model the dependence of this depolarization on the lidar FOV for different parameters of the scattering geometry. The corresponding results for the double-scattering approximation are presented in Figs. 14 and 15 below. The depolarization plotted in these figures is determined as a ratio $S_\perp/S_\parallel$, where $S_{\parallel,\perp}$ is calculated through Eq. (1), and the integration over the angle β is performed from 0 to θ. Figure 14 shows the depolarization of the laser radiation as a function of θ for different values of cloud base $z_a = 500$, 1000, and 2000 m. From Fig. 1, it is obvious that for the same sounding depth, the higher the cloud base, the larger the depolarization, because larger angles β will contribute to the scattered power. Figure 15 shows the angular dependence of the depolarization for $z_a = 1000$ m and different values of r_0. Depolarization rises with θ until it reaches a stable level, which slightly depends on the particle size: A change of r_0 from 5 to 50 μm decreases depolarization from 0.34 to 0.24. The larger the particle size, the smaller the range of θ where the depolarization rise occurs.

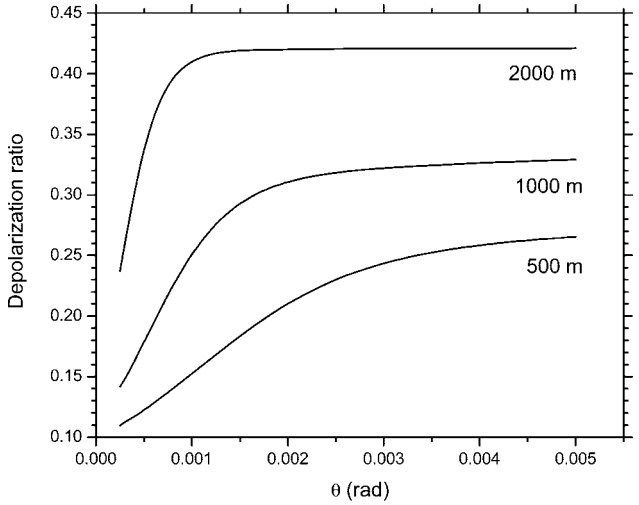

Fig. 14. Depolarization ratio $S_\perp/S_\parallel$ as a function of the FOV angle θ. Calculations are performed for $z_a = 500$, 1000, 2000 m and $\Delta z = 50$ m through Mie formulas. Size distribution is lognormal with $r_0 = 10$ μm.

4. Discussion

The increase of cloud base z_a shifts the angular distributions $s(\theta)$ toward small FOV, thus setting the limit to particle parameters that can be retrieved. So one of the principal applications of the MFOV technique might be to provide estimates of cloud particle size for altitudes up to several kilometers, which is typical for atmospheric clouds. To determine if this is a practical application, we calculated the minimum and maximum radii that satisfy the condition $l_{\min} > \varepsilon^2$ for different values of the parameter $\eta = \Delta z/z_a$. Figure 16 shows the dependence of the maximum and minimum particle radii on η. The results were calculated for the cross-polarized component, using eight FOVs distributed in the 0.25–5 mrad range with log-equidistant law and assuming a measurement uncertainty of $\varepsilon = 10\%$. The actual dependence is more complicated, but the approximation with a straight line gives the tendency. The sounding depth in clouds is quite limited if we want to avoid the effects of higher scattering orders; usually we have to keep it smaller than 100 m and, from Fig. 16, we can conclude that we cannot use $\eta < 0.01$ because $l_{\min} < 0.01$. This makes $z_a \sim 10{,}000$ m and the range of particle size $1 < r_0 < 4$ μm, which in general is insufficient. For lower clouds with $z_a \sim 5000$ m ($\eta = 0.02$), the interval of radii is much larger, i.e., $1.5 < r_0 < 25$ μm. Because many clouds in the atmosphere are located between a few hundred

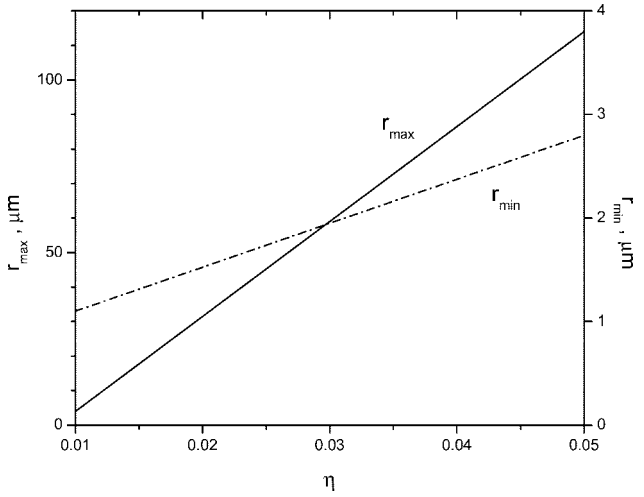

Fig. 16. Maximum and minimum particle radii that can be estimated from MFOV lidar measurements as functions of parameter $\eta = \Delta z/z_a$ for a measurement error $\delta < 10\%$. Results are obtained for eight FOVs in the 0.25–5 mrad range and for cross-polarized backscatter.

meters and 2–5 km, the MFOV lidar can effectively be used to study cloud microphysical parameters.

In fact, high-scattering orders have nonnegligible effects for optical depths higher than 0.5. Often, clouds have an extinction coefficient between 20 and 50 km^{-1}, and optical depths higher than 0.5 are reached within 10 to 25 m. One way to extend the sounding depth would be to subtract the high-scattering order contributions from the measured scattered power $S(\theta)$. This is precisely the method proposed by Roy *et al.*,[15] who make use of the azimuthal properties of the perpendicular polarization pattern produced by second-order scattering. The FOV-dependent perpendicular polarization pattern is measured with a gated intensified CCD camera for different depths in the cloud. The analysis of the images provides correction to the measured pattern for the contamination caused by scattering orders higher than 2. Another solution is the semi-empirical analytic model of the FOV dependence of multiply scattered lidar returns developed by Bissonnette *et al.*[5] This last model is valid for inhomogeneous clouds and optical depths as high as four.

It should also be noted that retrieval of cirrus cloud particle size has been done using single FOV high spectral resolution lidar[16] (HSRL) and Raman lidar[17] measurements. Although this technique is likely more limited than the MFOV technique due to the smaller amount of information available, it is attractive because the multiple-scattering information from cirrus clouds is available in most HSRL or Raman lidar measurements. Future efforts will focus on the use of the eigenvalue technique to study the information content of this MFOV particle size retrieval technique.

5. Conclusion

A methodology has been formulated to simulate and optimize lidar system design for the detection of multiply scattered signals. The detection of multiply scattered signals, while normally avoided in lidar measurements, can provide important information about cloud particle microphysics, including the particle size distribution. Our motivation for this work was to determine (i) what parameters can be retrieved using multiply scattered signals and (ii) what the optimal measurement geometry needed to retrieve the desired parameters is.

The simulations presented in this paper resolve the primary questions posed in the introduction:

- A MFOV lidar system should possess at least six FOVs. Further increasing the number of FOVs makes sense only if the uncertainty of the lidar measurements is better than 10%; otherwise it does not significantly increase the accuracy of particle size retrieval.
- For a wavelength of $\lambda = 1.06$ μm, the operational range $0.25 < \theta < 5$ mrad is sufficient to gain information about cloud particles and to separate the contributions of single- and double-scattering events. The use of smaller θ stabilizes the retrieval but poses complications to the lidar system design and operation. Optimal results are obtained when the FOVs are log-equidistantly distributed over this θ range.
- The retrieval results depend mainly on the ratio $\eta = \Delta z/z_a$, and the retrieval of particle size can be performed for η as small as ~0.02. For this η, the estimation of the particle size in the interval $1.5 < r < 25$ with an accuracy of ~30% is possible. The separation of the received scattered power for polarized and cross-polarized components significantly improves the retrieval and is always preferable.

All results of this paper were obtained for a double-scattering geometry, and the interference of higher scattering orders will lead to a degradation of the retrieval accuracy compared with what was derived here. The results presented are strictly applicable to small sounding depths in clouds and to thin aerosol layers. There are additional limitations related to the altitude dependence of the cloud parameters. These could be included in the analysis, but they are beyond the scope of the present paper. The investigation of how well a MFOV lidar technique will work for such situations is in our plans for future research.

For simplification of MFOV lidar design, it is desirable to decrease the maximal FOV. To compensate for a possible loss of information, use could be made of shorter wavelengths for the sounding (recall that FOV increase is equivalent to λ shortening). Such a combination of MFOV and multiwavelength lidars could have significant advantages compared with a single-wavelength lidar. Decreasing the maximal FOV in such a multiwavelength system should reduce the background signal. Moreover, the decrease of the FOV footprint on the cloud also makes the assumption of a flat cloud bottom more satisfactory.

It should also be mentioned that MFOV retrievals of the range-resolved extinction coefficient and the effective droplet diameter were successfully achieved in real clouds as reported in Ref. 5: The computations

were carried out automatically, no hand picking of data was made, and the success rate ranged from 100% in stable stratus conditions to ~50% in highly structured multilayered wispy clouds. Hence the MFOV lidar technique can handle complex natural clouds despite the seemingly restrictive assumptions made in constructing the retrieval method. Of course, field tests would have to be performed on the particular method of PSD retrieval discussed here.

The results obtained in this paper are only estimations, but they should be helpful for understanding the general features of the method and can be used as a guide for numerical simulations of the MFOV lidar performance and the practical MFOV lidar instrument design.

References

1. R. F. Cahalan, M. McGill, J. Kolasinski, T. Varnai, and K. Yetzer, "THOR—cloud thickness from offbeams lidar returns," J. Atmos. Ocean Technol. **22,** 605–627 (2005).
2. L. R. Bissonnette and D. L. Hutt, "Multiply scattered aerosol lidar returns: inversion method and comparison with *in situ* measurements," Appl. Opt. **34,** 6959–6975 (1995).
3. G. Roy, L. C. Bissonnette, C. Bastille, and G. Vallee, "Estimation of cloud droplet size density distribution from multiple-field-of-view lidar returns," Opt. Eng. **36,** 3404–3415 (1997).
4. G. Roy, L. Bissonnette, C. Bastille, and G. Vallee, "Retrieval of droplet-size density distribution from multiple-field-of-view cross-polarized lidar signals: theory and experimental validation," Appl. Opt. **38,** 5202–5211 (1999).
5. L. R. Bissonnette, G. Roy, and N. Roy, "Multiple-scattering-based lidar retrieval: method and results of cloud probing," Appl. Opt. **44,** 5565–5581 (2005).
6. I. Veselovskii, A. Kolgotin, D. Müller, and D. N. Whiteman, "Information content of multiwavelength lidar data with respect to microphysical particle properties derived from eigenvalue analysis," Appl. Opt. **44,** 5292–5303 (2005).
7. E. W. Eloranta, "Practical model for the calculation of multiply scattered lidar returns," Appl. Opt. **37,** 2464–2472 (1998).
8. P. Bruscaglioni, A. Ismaelli, and G. Zaccanti, "Monte Carlo calculations of lidar returns: procedure and results of Florence group," Appl. Phys. B **60,** 325–329 (1995).
9. I. L. Katsev, E. P. Zege, A. S. Prikhach, and I. N. Polonsky, "Efficient technique to determine backscattered light power for various atmospheric and oceanic sounding and imaging systems," J. Opt. Soc. Am. A **14,** 1338–1346 (1997).
10. C. Weikamp, ed., *Lidar: Range-Resolved Optical Remote Sensing of the Atmosphere,* Springer Series in Optical Science (Springer-Verlag, 2005), Chap. 3.
11. I. Polonskii, E. Zege, and I. L. Katsev, "Lidar sounding of warm clouds and determination of their microstructure parameters," Izv. Atmos. Oceanic Phys. **37,** 624–632 (2001).
12. F. B. Bohren and D. R. Huffman, *Absorption and Scattering of Light by Small Particles* (Wiley, 1983).
13. S. Twomey, ed., *Introduction to the Mathematics of Inversion in Remote Sensing and Direct Measurements* (Elsevier, 1977).
14. K. Sassen and H. Zhao, "Lidar multiple scattering in water droplet clouds: toward an improved treatment," Opt. Rev. **2,** 394–400 (1995).
15. N. Roy, G. Roy, L. R. Bissonnette, and J. R. Simard, "Measurement of the azimuthal dependence of cross-polarized lidar returns and its relation to optical depth," Appl. Opt. **43,** 2777–2785 (2004).
16. E. W. Eloranta and P. Piironen, "Measurements of particle size in cirrus clouds with the high spectral resolution lidar," in *Eighth International Workshop on Multiple Scattering Lidar Experiments, MUSCLE8, 98101,* Quebec, Canada, (1996).
17. D. N. Whiteman, K. D. Evans, B. Demoz, D. O'C. Starr, E. Eloranta, D. Tobin, W. Feltz, G. J. Jedlovec, S. I. Gutman, G. K. Schwemmer, M. Cadirola, S. H. Melfi, and F. J. Schmidlin, "Raman lidar measurements of water vapor and cirrus clouds during the passage of hurricane Bonnie," J. Geophys. Res. **106,** 5211–5225 (2001).